Supplementary Materials

Cytoplasmic Domain Filter Function in the Mechanosensitive Channel of Small Conductance

Ramya Gamini, Marcos Sotomayor, Christophe Chipot and Klaus Schulten

Movies

Movie S1. (movie-mscs.mpg) This movie shows the crystal structure (pdb:2OAU) of MscS (1, 2) with the TM domain embedded in the lipid bilayer. The seven subunits (P1 through P7) of MscS are shown in distinct colors. The TM pore, the distal pore and the seven side openings of the CD are displayed. The movie focuses at the end on one of the seven CD side openings revealing the amino-acid residues that line the opening and are distinguished by color: white, green, red and blue for non-polar, polar, negative and positive side groups, respectively.

Movie S2. (movie-abf.mpg) This movie shows the trajectory generated from ABF simulations `SimB` where Glu^- is translocated from the cytoplasmic to the interior side of the CD through one of the side openings. Glu^- is initally at location A of Fig. 3 and pauses at locations B, C, D and E (see also Fig. 3). Glu^- is shown to pass through the CD opening. Passing through the opening, Glu^- interacts with basic amino acids; Lys161 of subunit P7, Arg184 of subunit P6, as well as Arg238 and Arg185 of subunit P5. These interactions give rise to an enthalpic energy minimum in the PMF of Glu^- as shown in Fig. 3.

Figures

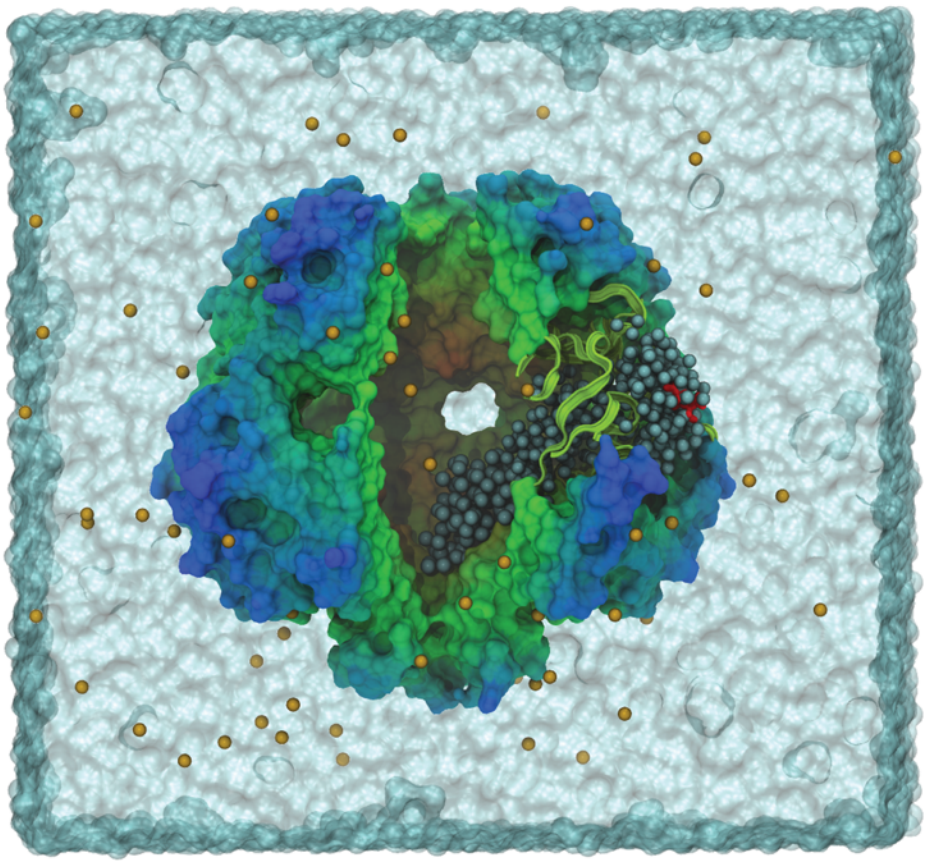

Figure S1: Flow of water through MscS cytoplasmic domain openings. Shown is the cytoplasmic domain protein in surface representation, cut open to expose the interior and colored from blue (outside) to green (middle) to brown (inside). On the right side of the domain, one of the openings is presented with the protein shown in ribbon representation to permit a view of water streaming through the opening, water being shown as blue spheres. K^+ ions are shown as gold spheres and a single Glu^- ion, colored in red, is shown surrounded by water in the right side opening. This figure illustrates that at any moment there are many water molecules available to stream through the domain openings while Glu^-, existing at much lower concentration than water, needs to find the domain openings. Surface-wise the openings are a small fraction ($\sim$1/50) of the domain outer surface.

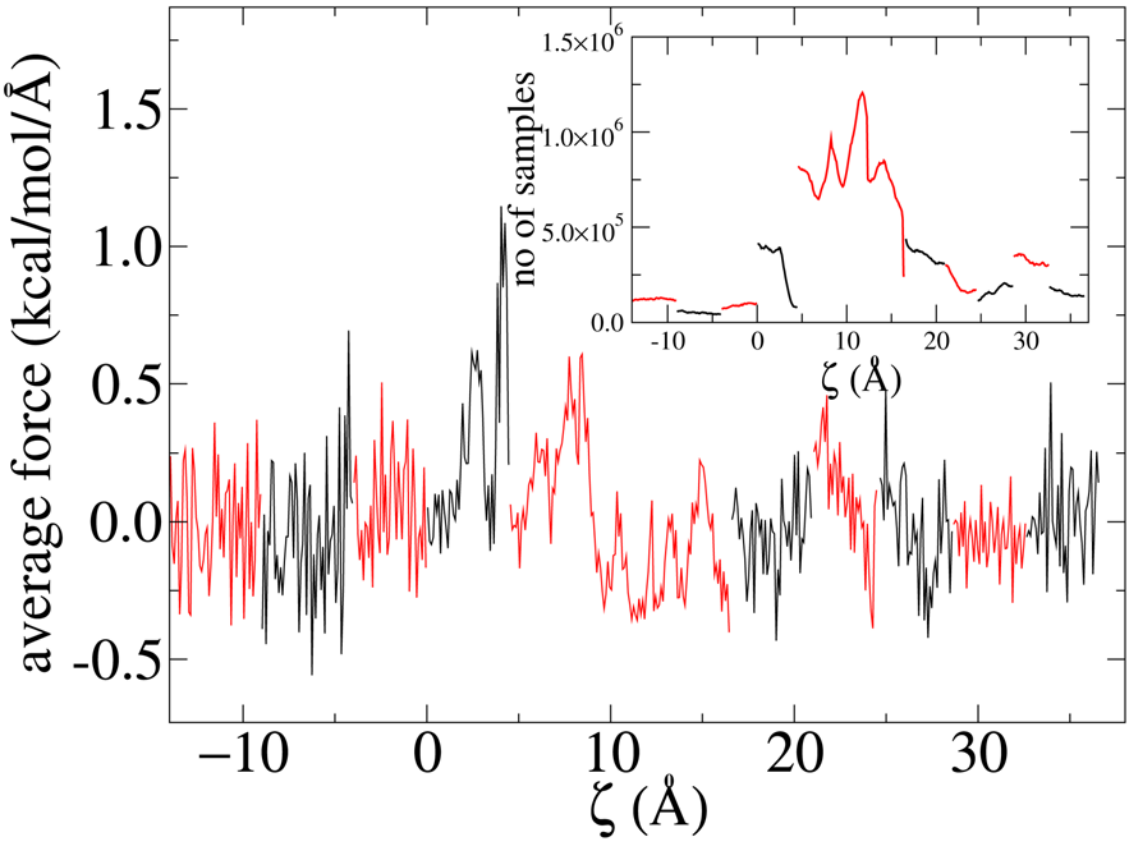

Figure S 2: Convergence of ABF simulation. Average forces across each of the 10 windows are shown to be continuous. The graph presents in its inset the sampling distribution in each window along the ζ-axis.

Molecular dynamics simulations. All molecular dynamics simulations were performed using NAMD 2.6 (3) with CHARMM27 parameters (4) and CMAP corrections (5). The TIP3P water model (6) was employed for water. The simulations were carried out in an NVT ensemble with the temperature maintained at 300 K using Langevin dynamics. During initial equilibration, NPT ensemble simulations were employed as noted, with a pressure maintained at 1 atm using a Nosé-Hoover Langevin piston (3). The simulations used multiple timestepping, with a base timestep of 1 fs, short-range interactions calculated every step, and long-range electrostatics every 2 steps. Electrostatic forces were evaluated through the particle-mesh Ewald method (3) with a grid density of 1.0 Å^{-3}. Periodic boundary conditions were assumed for all simulations. All MD trajectories were saved once per ps. Initial equilibration of `SimA` in the NPT ensemble covered 300 ps and of `SimB` 2000 ps. The equilibrium NVT ensemble simulations used a base timestep of 2 fs reaching a total sampling time of 380 ns for PMF calculations and of 14.3 ns for calculation of the electrostatic map.

Potential of mean force. To simulate the translocation of Glu^- through one of the side openings of the MscS CD, a Glu^- ion was initially positioned on the cytoplasmic side at a distance 51 Å away from the center of the CD along the line joining the center of the CD and the center of the side opening. For the purpose of evaluating the PMF of Glu^- along the translocation axis, the reaction coordinate, ζ, is defined as the distance of Glu^- from the center of the CD. Residues 158, 143, 243 and 247 of subunits P1 through P7 were chosen to define the center of the CD as the center of mass of these residues and residues 158, 143, 243 and 247 of subunit P6, lining the side opening, to define similarly the center of the side opening. In computing the reaction coordinate we chose only the carbonyl C atoms of the residues mentioned above to avoid contamination of the measured force due to holonomic constraints (7). To keep the Glu^- of interest from moving away from the side opening, an additional, cylindrical restraint was imposed along the translocation axis by attaching a virtual harmonic spring with spring constant 1.0 kcal mol^{-1} Å^{-2} to the backbone carbonyl C atom of this Glu^-, the constraint forces pointing towards the translocation axis passing through the middle of the CD opening. This restraint still allows the Glu^- ion to explore the whole volume of the opening.

ABF calculations were performed using 12 non-overlapping windows along the translocation axis, each of width 4-5 Å in which several ns of MD trajectory were generated. In addition, in cases where the average force was discontinuous across a bin barrier, further ABF calculations were run to convergence using the union of adjacent bins (across the three bins spanning the entire stretch of the side opening, from 5 Å to 20 Å). All PMF calculations were performed with the `SimB` set-up in the NVT ensemble assuming a Langevin damping coefficient of 1.0 ps^{-1}. Uniform sampling and continuity of average forces across the windows that demonstrate convergence of our ABF simulation is illustrated in Fig. S2.

Free-energy perturbation calculation

To examine the diffusion of K^+ from the bulk aqueous environment to the interior of the CD, a PMF could be generated in the spirit of the ABF calculation endeavored for Glu^-. However, this route has proven (for the case of Glu^-) to be computationally costly, in particular when, in the case of potassium, one is interested only at milestones along the reaction pathway — viz. points A, C and E, rather than the entire free-energy landscape. Accordingly, we resorted to an alternative numerical scheme for the K^+ PMF, namely, to calculate the free-energy change incurred in the replacement of Glu^- by K^+. Free-energy perturbation (8) (FEP) is particularly well suited to tackle this problem, wherein the anion located along the reaction pathway used in the computation of the PMF is mutated reversibly into its cationic counterpart, as depicted in Figure S3.

In the thermodynamic cycle depicted in Figure S3, in the left vertical transition Glu^- is transformed alchemically into K^+, both in the free state, i.e., in a 200 mM potassium glutamate bath in the absence of the CD. In case of the right side vertical transition the alchemical transformation occurs in association with CD. Our computational strategy involved calculating simultaneously the energy differences of the two vertical transitions, namely, $\Delta G^2_{\text{mut.}} - \Delta G^2_{\text{mut.}}$ and to calculate from this, through the identity $\Delta G^1_{\text{assoc.}} - \Delta G^2_{\text{assoc.}} = \Delta G^1_{\text{mut.}} - \Delta G^2_{\text{mut.}}$, the energy $\Delta G^1_{\text{assoc.}} - \Delta G^2_{\text{assoc.}}$ that yields the desired energy difference between Glu^- and K^+ in the side opening pathway. To increase the cost-effectiveness of the calculation of $\Delta G^2_{\text{mut.}} - \Delta G^2_{\text{mut.}}$, the two point mutations were performed concomitantly, the glutamate ion localized on the reaction pathway being replaced by its cationic counterpart, whilst symmetrically, a potassium ion lying sufficiently far away from the CD was transmuted into the corresponding anionic species. Aside from obviating the need to run separate simulations, concurrent alchemical transformation of a potassium and a glutamate ion in the same periodic cell circumvents size-consistency issues rooted in an incomplete treatment of long-range charge-dipole interactions (9), size-dependence corrections being mutually compensated here.

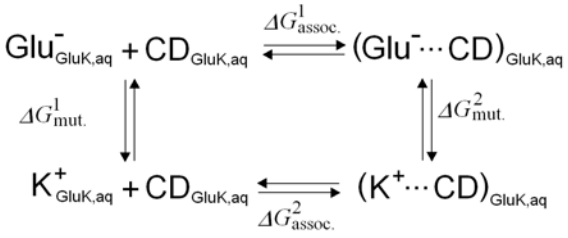

Figure S3: Thermodynamic cycle utilized to measure the free-energy change upon replacement by potassium of a glutamate ion. The horizontal legs of the cycle delineate the association of the ion, either glutamate or potassium, with the CD. The association free energy, $\Delta G^1_{\text{assoc.}}$, characterized by the upper, horizontal leg can be inferred from the PMF by integration of the latter (10). The vertical legs correspond to the point mutation of the anion in the free and in the bound states, so that $\Delta G^1_{\text{assoc.}} - \Delta G^2_{\text{assoc.}} = \Delta G^1_{\text{mut.}} - \Delta G^2_{\text{mut.}}$.

The position of the glutamate ion was restrained harmonically at points A and E as it was progressively transformed alchemically into the potassium ion. Conversely, at point C, the anion was free to diffuse radially in a thin, circular section, the radius of which was that of the pore.

point	ΔG (kcal/mol)	number of strata	time per stratum (ns)	total time (ns)
A	+0.2±0.3	100	0.096	9.60
C	+4.6±0.4	120	0.128	15.36
E	+0.2±0.4	100	0.096	9.60

Table S1: Stratification strategy and net free-energy change for the alchemical transformations into potassium of a glutamate ion located at three milestone positions of the potential of mean force characterizing the diffusion of the anion in and out of the CD. A potassium ion lying sufficiently far away from the CD is mutated concurrently into glutamate following the thermodynamic cycle of Figure S3.

The width of this section is equal to that of the bin used in the ABF calculation to accrue the instantaneous force acting along the reaction coordinate. Point mutations of the glutamate ion into the potassium ion was carried out in the framework of the dual-topology paradigm (11), wherein the reference and the target states of the transformation coexist without interacting mutually. The reaction pathway connecting these two states was stratified by means of 100 to 120 intermediate states, or strata, wherein up to 0.128 ns of sampling was performed, as summarized in Table S1. On account of the additional configurational entropy, convergence of the ensemble average required appreciably longer simulation time at point C than at points A and E. In each stratum, the first fourth of the sampling consisted of a thermalization of the molecular system prior to data collection. To alleviate singularities in the Lennard-Jones potential upon creation of the ions, either glutamate or potassium, a separation-shifted scaling scheme was employed (12), and van der Waals interactions were turned on prior to their electrostatic counterpart. The statistical error reflecting the precision of the free-energy calculation (13) was determined from the variance of the ensemble average. (14, 15) The correlation length of the time series was measured using the Flyvbjerg-Petersen renormalization group blocking method (16).

Calculation of the transmembrane conduction time τ_3.

In the following we will explain the mathematical expression stated in Eq. (36) of the main text. τ_3 describes how long it takes ions to leave the cytoplasmic domain through the open transmembrane channel to reach the extracellular space. Ion motion is controlled to a large degree by the cellular potential $U(x)$ which assumes a value V_o inside ($x < a$) the cell, zero outside ($x > a$) the cell and is close to constant in the cell interior. The potential varies from V_o to zero across the inner cellular membrane with a center position $x = a$. We assume here a sigmoidal variation of $U(x)$ inside the membrane with width σ. $U(x)$ is described through the function

$$U(x) \;=\; \frac{V_o}{2} \;-\; \frac{V_o}{2}\,\tanh[(x\,-\,a)/\sigma] \tag{1}$$

We assume also that the x-axis points along the center of the MscS channel in which case holds a = -16.86 Å and σ = 6 Å, the values having been determined through matching of expression (1) to the cellular potential calculated in (17). For the cell potential we assume V_o = -100 mV. We note that in applying $U(x)$ to Glu^- or K^+, one needs to multiply the potential with the sign of the ion charge, i.e., Glu^- experiences the potential $-\,U(x)$ as defined above, while K^+ experiences the potential $+\,U(x)$.

To determine τ_3 we will employ the mean first passage time description, as adopted also for calculation of τ_2. However, we need to account here for the narrowing of the cytoplasmic domain towards the transmembrane channel erecting an entropy barrier. To account for this barrier, at least qualitatively, we assume that diffusion orthogonal to the x-axis is more rapid than along the x-axis such that we can assume the distribution function for an ion, $p(x, y, z, t)$ to assume the form $\tilde{p}(x, t)\bar{p}_o(x|y, z)$ where $p_o(x|y, z)$ is the time-independent equilibrium distribution along y and z for fixed x. Integrating $\bar{p}(x, y, z, t)$ over the y- and z-coordinates yields $\bar{p}(x, t) \;=\; \tilde{p}(x, t)\, Z(x)$, where $Z(x)$ is the partition function in the y, z-plane. We assume here also that $\tilde{p}(x, t)$ corresponds to Brownian motion in the potential $U(x)$ stated above, i.e., at equilibrium $\tilde{p}(x, t) \;\propto\; \exp[-\beta U(x)]$. It should then hold $p(x, t \to \infty) \;\sim\; \exp[-\beta U(x)]\, Z(x) \;=\; \exp[-\beta\tilde{U}(x)]$ where $\tilde{U}(x) \;=\; U(x) \;-\; k_{\mathrm{B}}\mathrm{T}\ln Z(x)$.

The mean first passage time for the ions moving in the free energy $\tilde{U}(x)$ is then, according to Szabo et al. (18),

$$\tau_3 \;=\; \int_{x_{\mathrm{center}}}^{x_{\mathrm{out}}} dx D^{-1}(x) \exp[\beta\tilde{U}(x)] \int_{x_{\mathrm{apex}}}^{x} dx' \,\exp[-\beta\tilde{U}(x')] \tag{2}$$

Here x_{center} denotes the center of the cytoplasmic domain, x_{out} a position just outside of the transmembrane channel, i.e., just in the extracellular space, and x_{apex} the position at the apex of the cytoplasmic domain, i.e., the position inside the cytoplasmic domain widest from the transmembrane channel. Expression (2) can be employed to determine τ_3 once $Z(x)$ is specified. In the present case, $Z(x)$ is just the area of the cross section of the cytoplasmic domain and channel at point x along the x-axis, i.e., $Z(x) \;=\; \pi(r^2(x)/r_0^2)$, where $r(x)$ is the radius of the cross section along the symmetry axis, x, of the MscS and r_0 is a reference radius, the value of which drops out of the evaluation. We assume here that there is no obstacle impeding diffusion away or towards the x-axis.

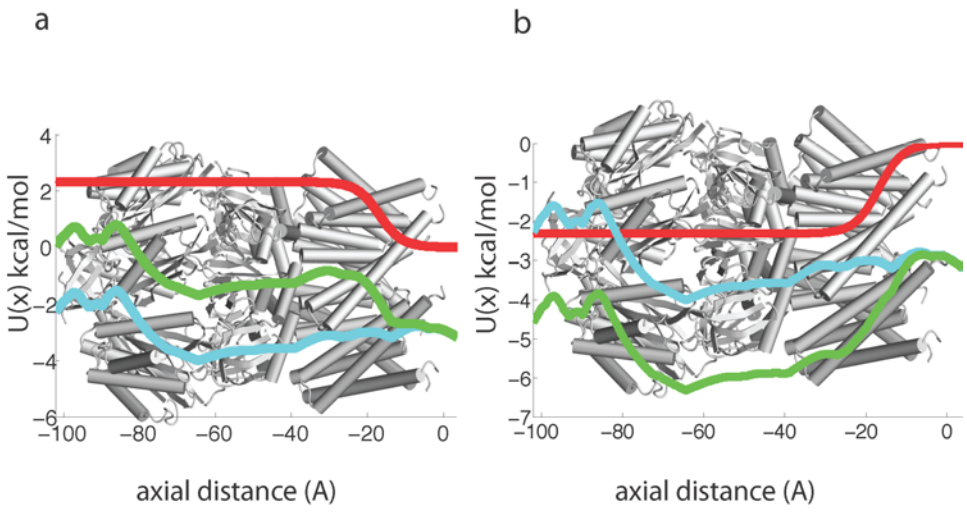

Figure S4: Comparision between the enthalpic and total potential for ions permeating along the symmetry axis of MscS. *(a)* Shown in red is the enthalpic potential $U(x)$, in blue $-k_{\mathrm{B}}\mathrm{T}\ln Z(x)$, and in green $\tilde{U}(x)$ for Glu^- permeating the transmembrane pore along the symmetry axis. *(b)* The corresponding potentials for K^+. MscS in its open conformation (PDB:2VV5) is shown in gray in both *(a)* and *(b)*.

Figure S4 compares the potentials $U(x)$, $-k_{\mathrm{B}}\mathrm{T}\ \ln Z(x)$ and $\tilde{U}(x)$ for Glu^- and K^+, showing that due to the presence of the spherical cytoplasmic domain the effective potential $\tilde{U}(x)$ develops a minimum at the domain center with a depth of about 4.0 $k_{\mathrm{B}}\mathrm{T}$. The origin of the minimum is the wider y, z-space available near the CD center than near the CD apex or the transmembrane channel.

Electrostatic energy of a "gas" of N_+ positive and N_- negative charges confined in a sphere at constant density. In the following we will demonstrate that the CD favors harboring an equal number of positive and negative osmolytes. We assume that N_+ positive and N_- negative ions are held inside the cytoplasmic domain at constant density, i.e., without correlation due to the mutual Coulomb attraction and repulsion or due to excluded volume effects. We define $N_+ = N + n$ and $N_- = N - n$ and we seek to determine the total Coulomb energy in case of a spherical cavity of radius R_o

$$E(N, n, R_o) \;=\; (\rho_{++} \;+\; \rho_{--} \;-\; \rho_{+-})\; I \tag{3}$$

where

$$\rho_{jk} \;=\; \rho_j\, \rho_k \tag{4}$$

and

$$I \;=\; \int d\vec{r}_1 \int d\vec{r}_2 \frac{1}{|\vec{r}_1 \;-\; \vec{r}_2|} \tag{5}$$

Here, $j,\, k = \pm$ and $\rho_\pm = 3\, e\, N_\pm/(4\,\pi\, R_o^3)$. I can be written $I = I_> + I_<$ where

$$I_> \;=\; \iint_{r_1 > r_2} \frac{1}{|\vec{r}_1 \;-\; \vec{r}_2|}\, d\vec{r}_1\, d\vec{r}_2 \tag{6}$$

and similarly for $I_<$. One can expand, following well known procedures (19),

$$I_> \;=\; \iint_{r_1 > r_2} d\vec{r}_1\, d\vec{r}_2\, \frac{1}{r_1} \sum_\ell \left(\frac{r_2}{r_1}\right)^\ell P_\ell(\cos\gamma) \tag{7}$$

where P_ℓ denotes the ℓ-th Legendre polynomial and γ the angle between $\vec{r}_1$ and $\vec{r}_2$. According to the addition theorem of spherical harmonics, $Y_{\ell m}$, one can write

$$P_\ell(\cos\gamma) \;=\; \frac{4\pi}{2\ell + 1} \sum_m Y^*_{\ell m}(\theta_1, \phi_1)\, Y_{\ell m}(\theta_2, \phi_2)\;; \tag{8}$$

here angles θ_j, ϕ_j define the direction of $\vec{r}_j$. The orthogonality relationships of the spherical harmonics lead to all terms in the sums to vanish, except the term with $\ell = 0$ and $m = 0$, such that one obtains, noting $Y_{00} = 1/\sqrt{4\pi}$,

$$I_> \;=\; 4\pi \iint_{r_1 > r_2} r_1^2 dr_1\; r_2^2 dr_2\; \frac{1}{r_1}\;. \tag{9}$$

One can readily derive

$$I_> \;=\; 4\pi R_o^5/15 \tag{10}$$

and also $I_> = I_<$. Altogether, one obtains finally

$$E(N, n, R_o) \;=\; \frac{3\, N^2}{10\,\pi}\, \frac{e^2}{R_o}\, \left[1 \;+\; 3\left(\frac{n}{N}\right)^2\right]\;. \tag{11}$$

The expression shows that the lowest energy arises for an equal number of positive and negative ions. The actual energy increase experienced in case of changing n from zero to one is $9e^2/10\,\pi\, R_o$,

but would be scaled down by the effective dielectric constant, ϵ, in the cytoplasmic domain. For $\epsilon = 1$ and $R_o = 43$ Å, the energy would be a few $k_{\rm B}$T. In reality, it should be less due to dielectric screening; however, the volume inside the CD available to ions might be characterized by a smaller R_o value; also the electrostatic energy in the CD would increase quadratically with n (excess number of positive over negative ions) and, hence, the interaction would likely favor significantly a balance of positive and negative ions in the cytoplasmic domain. Such balance would also be strengthened through correlation effects, e.g., through Glu^--K^+ pairing.

References

1. Bass, R. B., P. Strop, M. Barclay, and D. C. Rees. 2002. Crystal structure of *Escherichia coli* MscS, a voltage-modulated and mechanosensitive channel. *Science*. 298:1582–1587.

2. Steinbacher, S., R. B. Bass, P. Strop, and D. C. Rees. 2007. Structures of the prokaryotic mechanosensitive channels MscL and MscS. In O. P. Hamill, editor, *Current Topics in Membranes in Mechanosensitive Ion Channels, Part A*, volume 58. Elsevier Inc., New York, NY, pages 1–24.

3. Phillips, J. C., R. Braun, W. Wang, J. Gumbart, E. Tajkhorshid, E. Villa, C. Chipot, R. D. Skeel, L. Kale, and K. Schulten. 2005. Scalable molecular dynamics with NAMD. *J. Comp. Chem.* 26:1781–1802.

4. MacKerell Jr., A. D., B. Brooks, C. L. Brooks, III, L. Nilsson, B. Roux, Y. Won, and M. Karplus. 1998. CHARMM: The energy function and its parameterization with an overview of the program. In P. Schleyer et al., editors, *The Encyclopedia of Computational Chemistry*. John Wiley & Sons, Chichester, pages 271–277.

5. MacKerell, A. D., Jr., M. Feig, and C. L. Brooks III. 2004. Extending the treatment of backbone energetics in protein force fields: Limitations of gas-phase quantum mechanics in reproducing protein conformational distributions in molecular dynamics simulations. *J. Comp. Chem.* 25:1400–1415.

6. Jorgensen, W. L., J. Chandrasekhar, J. D. Madura, R. W. Impey, and M. L. Klein. 1983. Comparison of simple potential functions for simulating liquid water. *J. Chem. Phys.* 79:926–935.

7. Hénin, J. and C. Chipot. 2004. Overcoming free energy barriers using unconstrained molecular dynamics simulations. *J. Chem. Phys.* 121:2904–2914.

8. Zwanzig, R. W. 1954. High-temperature equation of state by a perturbation method. I. Nonpolar gases. *J. Chem. Phys.* 22:1420–1426.

9. Hummer, G., L. Pratt, and A. E. Garcia. 1996. Free energy of ionic hydration. *J. Phys. Chem.* 100:1206–1215.

10. Shoup, D. and A. Szabo. 1982. Role of diffusion in ligand binding to macromolecules and cell–bound receptors. *Biophys. J.* 40:33–39.

11. Gao, J., K. Kuczera, B. Tidor, and M. Karplus. 1989. Hidden thermodynamics of mutant proteins: A molecular dynamics analysis. *Science*. 244:1069–1072.

12. Zacharias, M., T. P. Straatsma, and J. A. McCammon. 1994. Separation-shifted scaling, a new scaling method for lennard-jones interactions in thermodynamic integration. *J. Chem. Phys.* 100:9025–9031.

13. Kofke, D. and P. Cummings. 1998. Precision and accuracy of staged free-energy perturbation methods for computing the chemical potential by molecular simulation. *Fluid Phase Equil.* 150:41–49.

14. Chipot, C. and A. Pohorille. 2007. *Free Energy Calculations. Theory and applications in chemistry and biology.* Springer Verlag.

15. Pohorille, A., C. Jarzynski, and C. Chipot. 2010. Good practices in free-energy calculations. *J. Phys. Chem. B.* (submitted).

16. Flyvbjerg, H. and H. G. Petersen. 1989. Error estimates on averages of correlated data. *J. Chem. Phys.* 91:461–466.

17. Sotomayor, M., V. Vasquez, E. Perozo, and K. Schulten. 2007. Ion conduction through MscS as determined by electrophysiology and simulation. *Biophys. J.* 92:886–902.

18. Szabo, A., K. Schulten, and Z. Schulten. 1980. First passage time approach to diffusion controlled reactions. *J. Chem. Phys.* 72:4350–4357.

19. Jackson, J. D. 1999. *Classical Electrodynamics 3rd ed.).* John Wiley & Sons, Inc, New York.